

A penalization method for calculating the flow beneath travelling water waves of large amplitude

A. Constantin, K. Kalimeris, O. Scherzer

RICAM-Report 2014-52

A penalization method for calculating the flow beneath travelling water waves of large amplitude

A. Constantin* K. Kalimeris† O. Scherzer ‡

November 19, 2014

Abstract

A penalization method for a suitable reformulation of the governing equations as a constrained optimization problem provides accurate numerical simulations for large-amplitude travelling water waves in irrotational flows and in flows with constant vorticity.

Keywords: Travelling water waves, vorticity, velocity field, pressure.

AMS Subject Classifications (2010): 35Q31, 35Q35, 76D33.

1 Introduction

Water flows with a uniform underlying current (possibly absent) are termed irrotational flows, while rotational waves describe the interaction of surface water waves with non-uniform currents. The study of the flow beneath an irrotational two-dimensional travelling surface wave in water with a flat bed is quite well-understood: see [5, 11] for theoretical studies, [4, 21] for numerical simulations and [3, 27] for experimental data. For rotational two-dimensional travelling water waves an existence theory for waves of large amplitude is available [10] and some numerical simulations were performed for flows without stagnation points [19, 20] and in the presence of stagnation points for flows of constant vorticity [26].

*Faculty of Mathematics, University of Vienna, Oskar-Morgenstern-Platz 1, 1090 Wien, Austria

†Radon Institute of Computational and Applied Mathematics, Altenberger Str. 69, 4040 Linz, Austria

‡Computational Science Center, University of Vienna, Oskar-Morgenstern-Platz 1, 1090 Wien, Austria, and Radon Institute of Computational and Applied Mathematics, Altenberger Str. 69, 4040 Linz, Austria

While water flows that originate in the state of irrotational flow are irrotational everywhere at all times thereafter (see [6]), a frequent occurrence of rotational flows is when non-uniform pure currents (with a flat free-surface) exist before the waves are generated and are disturbed by the waves. While the investigation of the resulting wave-current interaction is quite intricate, within the framework of two-dimensional flows the vorticity of a particle is preserved as the particle moves about (see [6]), and this structural property permits us to classify in such a setting rotational flows in terms of their vorticity distribution. A pure current in a two-dimensional flow over a flat bed is represented by a vanishing vertical fluid velocity component and a depth-dependent horizontal fluid velocity component, the gradient of which is the vorticity. Consequently, uniform currents correspond to zero vorticity (irrotational flow), while the simplest example of non-uniform currents are flows with constant non-zero vorticity. The most regular and predictable currents are the tidal currents, and they are the most significant currents on areas of the continental shelf and in many coastal inlets [18]. Tidal currents are the alternating horizontal movements of water associated with the rise and fall of the tide: the current associated with a rising tide, called the flood, and the current associated with a falling tide, called the ebb. Positive constant vorticity $\omega > 0$ is appropriate for the modelling of the ebb current and negative constant vorticity $\omega < 0$ for the flood current, cf. the discussion in [6, 14]. On the other hand, the prime source of some ocean currents like the Agulhas current and the Gulf Stream are long-duration winds, and a depth-dependent vorticity rather than constant vorticity is adequate to describe such currents. Also, the out-flowing current at the mouth of an estuary generally exhibits a non-uniform vorticity distribution, cf. [18].

While in some engineering applications attempts were made to approximate rotational wave-current interactions by waves interacting with a suitably chosen uniform underlying current, there are major pitfalls associated with such an approach [25]. Experimental results (see [23, 24]) demonstrate the importance of the global vorticity distribution in the study of wave-current interactions. The governing equations for two-dimensional travelling waves take on the form of a planar nonlinear elliptic free-boundary problem in a frame moving at the wave speed (see Section 2 below). In the irrotational case this problem can be re-formulated as a boundary integral equation and numerical simulations of the solutions can be obtained by means of discretizations. The applicability of the boundary integral methods is not restricted to small perturbations of a flat free surface but hinges on the knowledge of analytical expressions for the kernel of the integral operators, a feature that reduces its scope. Other than irrotational flows, boundary

integral methods can be used for flows with constant vorticity since in this setting the problem can be reduced to a nonlinear free-boundary problem for Laplace's equation by subtraction of the particular solution $\frac{1}{2}\omega y^2$; see [14, 28]. Let us also point out that for flows of constant vorticity somewhat different, but nevertheless related, analytical re-formulations of the governing equations rely on the Dirichlet-Neumann operator methodology [1, 2, 13, 12]. However, all these approaches are ineffective in dealing with a continuous non-constant vorticity distribution. The present paper is devoted to two important issues of the numerical simulation of rotational water waves. The first regards the possibility of implementing a numerical approach that is not restricted to flows with a uniform distribution of vorticity, and the second concerns the possibility of an efficient way to select from the plethora of solutions those representing waves of large amplitude. In particular, it is desirable to concentrate on genuine waves by avoiding pure currents (with a flat free surface). We will provide an approach that addresses both issues for wave-current interactions without flow reversals. For most laboratory experiments the wave speed c is typically an order of magnitude greater than the maximum of the horizontal component u of the velocity field (u, v) , cf. [25]. However, strong adverse currents can produce flows with critical layers and stagnation points – curves (in the moving frame) along which $u = c$ and points where $u = c$ and $v = 0$, respectively. The absence of critical layers and stagnation points ensures that no flow-reversal occurs and in this case a hodograph transform permits the re-formulation of the governing equations, in a frame of reference moving at the wave speed, as a nonlinear oblique boundary-value problem for a quasi-linear elliptic partial differential equation in a fixed rectangular domain, cf. [10]. Among the solutions of this equivalent form we have laminar flows (pure currents with a flat free surface and with $v \equiv 0$ throughout the fluid) as well as genuine waves. Field data and laboratory measurements show that, unless we deal with a small perturbation of a flow with a flat free surface, the physical flow parameters wavelength, wave speed, relative mass flux, and wave energy do not determine uniquely the specific wave motion. Pure currents correspond to solutions that are independent of the horizontal coordinate, irrespective whether they are considered in the moving frame or after performing the hodograph transform. To select waves of large amplitude we impose the constraint of maximizing the L^2 -norm of the slope of the wave profile, over one wavelength. We propose a penalization method to solve numerically this constrained optimization problem in the fixed rectangular domain. This permits us to provide accurate simulations of the surface water wave but

also of the main flow characteristics (fluid velocity components, pressure) beneath it. While our approach can be adapted to investigate wave-current interactions in flows with non-constant vorticity, we nevertheless choose to illustrate it on flows with a uniform vorticity distribution. On one hand, the assumption of constant vorticity is attractive for analytical tractability. More importantly, this setting permits us to show that our approach is sufficiently accurate to capture features of the free surface profile that mark the contrast with irrotational flows and were highlighted in experimental studies. These features of the wave profile are also attainable by relying on the boundary integral method rather than discretizing the bulk, but in gathering information about the flow beneath the waves the computational advantage of the boundary integral methods, due to the reduction of the dimension of the problem by one, becomes less relevant as the issue of the dynamics in the interior of the fluid domain has also to be addressed.

Concerning the practical relevance of our considerations, let us note that while flow reversal occurs in tidal currents and there are periods of “slack water” when there is little or no horizontal motion, over extended time the flow is uni-directional. For example, the tidal currents through Cook Strait between the two main islands of New Zealand is daily in one direction for about 6 h and in the reverse direction for another 6 h. While the Cook Strait, 30-40 km long and 23 km wide at its narrowest point, has a particularly irregular bottom topography near the shores, making it one of the most dangerous and unpredictable waters in the world, there is an extensive submarine plateau at 140 m depth. The tidal currents here reach speeds up to 3.6 m/s and surface waves exceeding 10 m in wave height can be observed, with wavelengths around 150 m; wave height being defined as the overall vertical change in height between the highest elevation of the wave and the lowest depression. Measurements of the profile of the current velocity profile indicate the range of within 0.3 m/s for the vertical variations in magnitude over the water column [29]. Let us also point out that that tidal currents can reach speeds up to a startling 5.5 m/s in between the Scottish mainland and the Orkney Islands in the Pentland Firth. In the Inner Sound at this location, away from the coast, the sea bed is almost flat over an area several km long and more than 1 km wide, at a depth of about 35 m. Wave heights of 4 m are common and typical values of the vorticity of the tidal currents are $\gamma \approx \pm 0.03 \text{ s}^{-1}$, so that the current speed difference between surface and bed is about 1 m/s. Measurements also show that the mean current speeds are in the range of $\pm 3 \text{ m/s}$ during the 5 h long flood tide and the 5 h long ebb tide, when the water moves from west to east and from east to west, respectively, with no flow reversal, cf. [17].

2 Preliminaries

In this section we present the governing equations for periodic two-dimensional travelling water waves in a flow of constant vorticity over a flat bed. We also briefly discuss their reformulation, used in [10] to show, by means of bifurcation theory, the existence of waves of small and large amplitude.

2.1 Steady two-dimensional water waves

Let us first discuss the governing equations for two-dimensional waves travelling at constant speed and without change of shape at the surface of a layer of water above a flat bed, in a flow of constant vorticity. Two-dimensionality means that the waves propagate in a fixed horizontal direction, say X , and the flow presents no variation in the horizontal direction orthogonal to the direction of wave propagation. For this reason, it suffices to analyse a vertical cross-section of the flow, parallel to the direction of wave propagation. To model sea waves of large amplitude the assumptions of inviscid flow in a fluid of constant density are appropriate and the effects of surface tension are negligible – see the discussion in [6]. The assumption of a flat bed $Y = -d$ is also reasonable for a considerable proportion of the Earth’s sea floor, due to the fact that abyssal plains (sediment-covered regions that are the flattest areas on Earth, with slopes that do not exceed 10^{-4}) cover almost half of the Earth’s total sea floor. Consequently, the cross-section of the fluid domain is of the form

$$\mathcal{D}(t) = \{(X, Y) : X \in \mathbb{R} \text{ and } -d < y < \xi(X - ct)\},$$

where $c > 0$ is the wave speed, $d > 0$ is the average depth and ξ is the profile of the free surface that oscillate around the flat free surface $Y = 0$, that is

$$\int_0^L \xi(X - ct) dX = 0, \tag{2.1}$$

at any fixed time t , $L > 0$ being the wavelength. Setting the density of the water $\rho \equiv 1$, the incompressible Euler equations for the velocity field $(U(X - ct, Y), V(X - ct, Y))$ and the pressure $P(X - ct, Y)$ are

$$\begin{cases} U_X + V_Y = 0, \\ (U - c)U_X + VU_Y = -P_X, \\ (U - c)V_X + VV_Y = -P_Y - g, \end{cases} \quad \text{in } \mathcal{D}(t), \tag{2.2}$$

where g is the gravitational constant of acceleration. The boundary conditions that select the water waves from the solutions to (2.2) are

$$\begin{cases} P = P_{atm} & \text{on } Y = \xi(X - ct), \\ V = (U - c)\xi_x & \text{on } Y = \xi(X - ct), \\ V = 0 & \text{on } Y = -d, \end{cases} \quad (2.3)$$

where P_{atm} is the constant atmospheric pressure. The first condition in (2.3) reflects the fact that surface tension effects are negligible and permits the decoupling of the water motion from the air flow above it, the density of the air being 10^{-3} times that of the water. The second and third conditions in (2.3) express the fact that the free surface and the flat bed are interfaces, with no flow possible across them – see the discussion in [6].

Since the flow is periodic in the X -variable, for computational convenience we will assume that the normalized period is 2π . To translate our results into physically relevant quantities, note that for a wave of wavelength L , the change of variables (scaling)

$$\begin{aligned} \tilde{X} &= \kappa X, & \tilde{Y} &= \kappa Y, & \tilde{U} &= U, & \tilde{V} &= V, & \tilde{t} &= \kappa t, \\ \tilde{\xi} &= \kappa \xi, & \tilde{c} &= c, & \tilde{P} &= P, & \tilde{g} &= \kappa^{-1} g, & \tilde{d} &= \kappa d, \end{aligned} \quad (2.4)$$

expressed in terms of the (non-dimensional) parameter $\kappa = \frac{2\pi}{L}$, has the effect that the new variables (dependent and independent) satisfy a periodic system in the tilded variables of a form almost identical to (2.2)-(2.3), the only difference being that g should be replaced by \tilde{g} in (2.2). For practical purposes it is useful to keep track of the way two important physical flow parameters behave under this scaling: the relative mass flux (relative to the uniform flow at speed c)

$$M = \int_{-d}^{\xi(X-ct)} [U(X-ct, Y) - c] dY,$$

expression that can be seen to be independent of $(X - ct)$ due to the first equation in (2.2) and to the last two relations in (2.3), and the vorticity

$$\omega = U_Y - V_X$$

that is the hallmark of underlying currents. We have

$$\tilde{M} = \kappa M, \quad \omega = \kappa \tilde{\omega}. \quad (2.5)$$

The practical significance of the scaling (2.4) is that a normalized wave motion with wavelength 2π m, relative mass flux $2 \text{ m}^2/\text{s}$ and vorticity 1 s^{-1}

corresponds, due to (2.5), to a relative mass flux of the order of $67 \text{ m}^2/\text{s}$ and vorticity $\omega \approx 0.03 \text{ s}^{-1}$ for physically realistic wavelengths of the order $L \approx 210 \text{ m}$.

In a frame moving at the (constant) wave speed, obtained by means of the change of variables

$$x = X - ct, \quad Y = y,$$

we can restrict our attention to the two-dimensional bounded domain

$$\mathcal{D} = \{(x, y) : -\pi < x < \pi \text{ and } -d < y < \eta(x)\},$$

bounded above by the free surface profile

$$S = \{(x, y) : -\pi < x < \pi \text{ and } y = \eta(x)\},$$

and below by the flat bed

$$B = \{(x, y) : -\pi < x < \pi \text{ and } y = -d\},$$

where $\eta(x) = \xi(X - ct)$. Setting

$$u(x, y) = U(X - ct, y), \quad v(x, y) = V(X - ct, Y), \quad \mathfrak{p}(x, y) = P(X - ct, Y),$$

(2.2) can be written as

$$\begin{cases} u_x + v_y = 0, \\ (u - c)u_x + vu_y = -\mathfrak{p}_x, \\ (u - c)v_x + vv_y = -\mathfrak{p}_y - \tilde{g}, \end{cases} \quad \text{in } \mathcal{D}, \quad (2.6)$$

while (2.3) read as follows

$$\begin{cases} \mathfrak{p} = P_{atm} \text{ on } S, \\ v = (u - c)\eta_x \text{ on } S, \\ v = 0 \text{ on } B. \end{cases} \quad (2.7)$$

We denote by

$$\gamma = u_y - v_x$$

the normalized vorticity.

Throughout this paper we restrict our attention to flows for which

$$u < c \quad \text{throughout the fluid}, \quad (2.8)$$

condition that prevents the appearance of stagnation points in the flow and the occurrence of flow-reversals.

2.2 Stream function formulation

Structural properties of the governing equations (2.6)-(2.7) enable us to reduce the number of unknowns. Note first that the relative mass flux

$$p_0 = \int_{-d}^{\eta(x)} (u(x, y) - c) dy < 0, \quad (2.9)$$

due to (2.8). The first equation in (2.6) permits us to introduce the stream function $\psi(x, y)$ as the unique solution of the differential equations

$$\psi_x = -v \quad \text{and} \quad \psi_y = u - c \quad \text{in } \overline{\mathcal{D}}, \quad (2.10)$$

subject to

$$\psi(x, -d) = -p_0. \quad (2.11)$$

Note that $\psi(x, y)$ is periodic in the x -variable, and that the third equation in (2.7) is consistent with the constraint (2.11). Moreover, (2.10) and the definition of vorticity yield

$$\Delta\psi = \gamma \text{ in } \mathcal{D}. \quad (2.12)$$

The first equation in (2.7) is equivalent to ψ being constant on S , while (2.9) together with (2.11) ensure that this constant must vanish, that is,

$$\psi = 0 \text{ on } S. \quad (2.13)$$

On the other hand, due to (2.10), we see that we can re-express the Euler equation in (2.6) by the fact that the expression $\frac{(u-c)^2+v^2}{2} + \tilde{g}y + \mathbf{p} - \gamma\psi$ equals a constant E throughout \mathcal{D} , this being a form of conservation of energy (see [6]). Consequently, the governing equations (2.6)-(2.7) can be reformulated in terms of the stream function as the free-boundary problem

$$\begin{cases} \Delta\psi = \gamma & \text{in } \mathcal{D}, \\ \psi = 0 & \text{on } S, \\ \psi = p_0 & \text{on } B, \\ \frac{|\nabla\psi|^2}{2} + \tilde{g}y = Q & \text{on } S, \end{cases} \quad (2.14)$$

where $Q = E - P_{atm}$, $p_0 < 0$ and γ are constants. Given p_0 , we seek values of d and Q for which (2.14) admits a smooth solution $\psi(x, y)$, even and of period 2π in the x -variable. Evenness reflects the requirement that u and η are symmetric while v is anti-symmetric about the crest line $x = 0$; here, we shift the moving frame to ensure that the wave crest is located at $x = 0$. Symmetric waves present these features and it is known that a solution with a free surface S that is monotone between successive crests and troughs has to be symmetric, cf. [8].

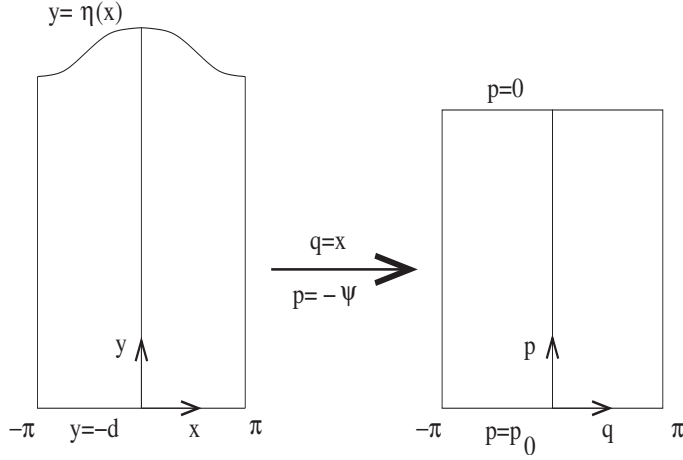


Figure 1: Dubreil-Jacotin transformation

2.3 Hodograph transform

Under the assumption (2.8), a partial hodograph transform leads to a reformulation of the free-boundary problem (2.14) as a nonlinear oblique boundary-value problem for a quasilinear elliptic partial differential equation in a known strip. In this process, the normalized gravitational constant \tilde{g} , the relative mass flux p_0 and the constant vorticity γ are considered to be known, while the average depth d and the hydraulic head Q are allowed to vary to accommodate the existence of a flow.

The assumption (2.8) and the definition of the stream function (2.10) yield that $\psi(x, y)$ is a strictly decreasing function of y throughout the fluid domain \mathcal{D} , being periodic in the x -variable. Moreover, due to (2.11) and (2.13), ψ is constant both on the bottom B and on the free surface S . The Dubreil-Jacotin transformation [15]

$$q = x, \quad p = -\psi,$$

transforms the unknown domain \mathcal{D} to the rectangle

$$R = \{(q, p) : -\pi < q < \pi, p_0 < p < 0\}, \quad (2.15)$$

(see Figure 1). Let

$$h(q, p) = y + d \quad (2.16)$$

be the height above the flat bottom B . Since ψ is a strictly decreasing function of y , for every fixed x the height h above the flat bottom is a single

valued function of ψ (or, equivalently, p), with

$$\begin{cases} h_q = \frac{v}{u-c}, & h_p = \frac{1}{c-u}, \\ v = -\frac{h_q}{h_p}, & u = c - \frac{1}{h_p}, \end{cases} \quad (2.17)$$

and, more generally,

$$\begin{cases} \partial_x = \partial_q - \frac{h_q}{h_p} \partial_p, & \partial_y = \frac{1}{h_p} \partial_p, \\ \partial_p = \frac{1}{c-u} \partial_y, & \partial_q = \partial_x - \frac{v}{c-u} \partial_y. \end{cases} \quad (2.18)$$

Using the change of variables relations (2.18), we get that

$$\begin{aligned} \gamma &= \partial_y u - \partial_x v = \frac{1}{h_p} \partial_p \left(c - \frac{1}{h_p} \right) - \left(\partial_q - \frac{h_q}{h_p} \partial_p \right) \left(-\frac{h_q}{h_p} \right) \\ &= \frac{h_{pp}}{h_p^3} - \frac{-h_p h_{qq} + h_q h_{pq}}{h_p^2} + \frac{-h_p h_q h_{pq} + h_q^2 h_{pp}}{h_p^3}, \end{aligned}$$

while

$$|\nabla \psi|^2 = v^2 + (u-c)^2 = \frac{1 + h_q^2}{h_p^2}.$$

These considerations show that the constitutive equations for the height function $h(q, p)$, which is even and 2π -periodic in q , are

$$\begin{cases} \mathcal{H}[h] := (1 + h_q^2) h_{pp} - 2h_p h_q h_{pq} + h_p^2 h_{qq} - \gamma h_p^3 = 0 & \text{on } R, \\ \mathcal{B}_0[h] := 1 + h_q^2(q, 0) + (2\tilde{g}h - Q) h_p^2(q, 0) = 0, \\ \mathcal{B}_1[h] := h(q, p_0) = 0. \end{cases} \quad (2.19)$$

In the new formulation (2.19), the wave profile $\eta(x)$ is given by $h(q, 0)$, the wave height being the difference

$$\max_{q \in [-\pi, \pi]} h(q, 0) - \min_{q \in [-\pi, \pi]} h(q, 0). \quad (2.20)$$

while half of (2.20) represents the wave amplitude.

3 Laminar Flow and Linearized Equations

The simplest solutions are the laminar flows with a flat free surface, representing pure currents. Near such flows a linearization procedure permits us

to obtain the first-order approximations of genuine water waves, provided that such waves exist – a fact that depends on the specific values of the physical flow parameters that are involved (see below). These linear waves capture well the characteristics of waves of small amplitude.

3.1 Laminar flows

Let us discuss the solutions describing parallel shear flows, with $\eta \equiv 0$. In this case the solution h of (2.19) is independent of q : $h(q, p) = H(p)$ with

$$\begin{cases} \mathcal{H}_L[H] := H_{pp} - \gamma H_p^3 = 0 \text{ in } R, \\ \mathcal{B}_{L,0}[H] := 1 + (2\tilde{g}H(0) - Q)H_p^2(0) = 0, \\ \mathcal{B}_{L,1}[H] := H(p_0) = 0. \end{cases} \quad (3.1)$$

The explicit solution of (3.1) is given by

$$H(p; \lambda) = \frac{2(p - p_0)}{\sqrt{\lambda - 2\gamma p} + \sqrt{\lambda - 2\gamma p_0}}, \quad p_0 \leq p \leq 0, \quad (3.2)$$

provided that the parameter $\lambda > 0$ satisfies the equation

$$Q = \lambda + \frac{4\tilde{g}|p_0|}{\sqrt{\lambda} + \sqrt{\lambda - 2\gamma p_0}}. \quad (3.3)$$

3.2 Linearized Solutions

We now present the outcome of the linearization of the system (2.19) near the laminar flow $H(p)$.

We consider a parametrized family of functions of the form

$$\hat{h}(q, p) = H(p) + bm(q, p), \quad (3.4)$$

where $b \in \mathbb{R}$ and the function m is even and 2π -periodic in q , such that

$$\mathcal{H}[\hat{h}](p, q) = \mathcal{O}(b^2), \quad \mathcal{B}_0[\hat{h}](q) = \mathcal{O}(b^2) \text{ and } \mathcal{B}_1[\hat{h}](q) = 0. \quad (3.5)$$

Taking the definition of $\mathcal{H}, \mathcal{B}_0, \mathcal{B}_1$ from (2.19) into account, we find that $\mathcal{H}[\hat{h}](p, q)$ is given by

$$\begin{aligned} & (1 + H_q^2(p) + 2bH_q(p)m_q(q, p) + b^2m_q(q, p))(H_{pp}(p) + bm_{pp}(p, q)) \\ & - 2(H_p(p) + bm_p(q, p))(H_q(p) + bm_q(q, p))(H_{pq}(p) + bm_{pq}(p, q)) \\ & + (H_p^2(p) + 2bH_p(p)m_p(p, q) + b^2m_p^2(p, q))(H_{qq}(p) + bm_{qq}(p, q)) \\ & - \gamma(H_p^3(p) + 3bm_p(p, q)H_p(p) + \mathcal{O}(b^2)). \end{aligned}$$

Using the fact that $H_q = 0$, the expression for $\mathcal{H}[\hat{h}](p, q)$ simplifies to

$$\begin{aligned}
& (1 + b^2 m_q(q, p))(H_{pp}(p) + b m_{pp}(p, q)) \\
& - 2b^2 (H_p(p) + b m_p(q, p) m_q(q, p) m_{pq}(q, p)) \\
& + b (H_p^2(p) + 2b H_p(p) m_p(p, q) + b^2 m_p^2(p, q)) m_{qq}(p, q) \\
& - \gamma (H_p^3(p) + 3b m_p(p, q) H_p^2(p) + \mathcal{O}(b^2)) \\
& = H_{pp}(p) - \gamma H_p^3(p) \\
& + b (m_{pp}(p, q) + H_p^2(p) m_{qq}(p, q) - 3\gamma m_p(p, q) H_p^2(p)) + \mathcal{O}(b^2) .
\end{aligned}$$

Similarly,

$$\begin{aligned}
\mathcal{B}_0[\hat{h}](q) &= 1 + (2\tilde{g}H(0) - Q)H_p^2(0) \\
& + b2H_p(0) ((2gH(0) - Q)m_p(q, 0) + \tilde{g}H_p(0)m(q, 0)) + \mathcal{O}(b^2) .
\end{aligned}$$

Using the fact that (3.1) and (3.2) yield $H_p(0) = \frac{1}{\sqrt{\lambda}}$ and $2\tilde{g}H(0) - Q = -\lambda$, we infer that

$$\begin{aligned}
\mathcal{B}_0[\hat{h}](q) &= 1 + (2\tilde{g}H(0) - Q)H_p^2(0) \\
& + b\frac{2}{\lambda} \left(-\lambda^{3/2} m_p(q, 0) + \tilde{g}m(q, 0) \right) + \mathcal{O}(b^2) .
\end{aligned}$$

H being a solution to (3.1) shows that \hat{h} solves (3.5) if and only if m satisfies the linearised system

$$\begin{cases} m_{pp} + H_p^2 m_{qq} = 3\gamma H_p^2 m_p \text{ in } R, \\ \tilde{g}m(q, 0) = \lambda^{3/2} m_p(q, 0) \text{ for } -\pi < q < \pi, \\ m(q, p_0) = 0 \text{ for } -\pi < q < \pi. \end{cases} \quad (3.6)$$

For a general value of $\lambda > 0$, the problem (3.6) will admit only the trivial solution $m \equiv 0$. However, specific values of λ produce non-trivial solutions:

- In the irrotational case $\gamma \equiv 0$ we have that the solution to (3.1) is

$$H(p; \lambda) = \frac{p - p_0}{\sqrt{\lambda}}, \quad (3.7)$$

and the non-trivial solution of the linearized equations (3.6) is given by $m(q, p) = M(p) \cos(q)$ with

$$M(p) = \sinh\left(\frac{p - p_0}{\sqrt{\lambda^*}}\right), \quad (3.8)$$

where $\lambda^* > 0$ satisfies the dispersion relation

$$\lambda + \tilde{g} \tanh\left(\frac{p_0}{\sqrt{\lambda}}\right) = 0, \quad (3.9)$$

the corresponding value of Q being $Q^* = \lambda^* - \frac{2\tilde{g}p_0}{\sqrt{\lambda^*}}$. We obtain the linear solution

$$h^*(q, p; b) = \frac{p - p_0}{\sqrt{\lambda^*}} + b \cos q \sinh\left(\frac{p - p_0}{\sqrt{\lambda^*}}\right), \quad (3.10)$$

with b constant. This is the first-order approximation to the solution of the problem (2.19), up to order $\mathcal{O}(b^2)$, for small enough b . In terms of the mean depth d , note that $H(0) = d$, so that (3.7) yields $d\sqrt{\lambda^*} = -p_0$ and (3.9) reads

$$\sqrt{\lambda^*} = \sqrt{\tilde{g} \tanh(d)}. \quad (3.11)$$

Recall that $\sqrt{\lambda^*}$ is the speed of the bifurcating laminar flow at its (flat) free surface, since $H_p(0) = \frac{1}{\sqrt{\lambda^*}}$.

- Similarly, in the case of constant non-zero vorticity γ , for

$$Q^* = \lambda^* - \frac{4\tilde{g}p_0}{\sqrt{\lambda^*} + \sqrt{\lambda^* - 2p_0\gamma}}$$

we get the linear solution

$$h^*(q, p; b) = H^*(p) + b \cos q M(p), \quad (3.12)$$

with

$$H^*(p) = \frac{2(p - p_0)}{\sqrt{\lambda^* - 2\gamma p} + \sqrt{\lambda^* - 2\gamma p_0}} \quad (3.13)$$

and

$$M(p) = \frac{1}{\sqrt{\lambda^* - 2p\gamma}} \sinh\left(\frac{2(p - p_0)}{\sqrt{\lambda^* - 2\gamma p} + \sqrt{\lambda^* - 2\gamma p_0}}\right), \quad (3.14)$$

where $\lambda^* > 0$ is the solution of the dispersion relation

$$\frac{\lambda}{g - \gamma\sqrt{\lambda}} + \tanh\left(\frac{2p_0}{\sqrt{\lambda} + \sqrt{\lambda - 2p_0\gamma}}\right) = 0. \quad (3.15)$$

Since $H(0) = d$, we can write (3.15) in the form $\frac{\lambda}{g - \gamma\sqrt{\lambda}} + \tanh(d)$, so that

$$\sqrt{\lambda^*} = -\frac{\gamma \tanh(d)}{2} \pm \sqrt{\frac{\gamma^2 \tanh^2(d)}{4} + \tilde{g} \tanh(d)}, \quad (3.16)$$

where $\sqrt{\lambda^*}$ is the speed of the bifurcating laminar flow at its (flat) free surface. Setting $\gamma = 0$ in (3.16) we recover (3.11). The dispersion relation (3.16) also hints at a difference between the cases of positive and negative constant vorticity. Indeed, (3.15) has a unique solution $\lambda \in \left(0, \frac{\tilde{g}^2}{\gamma^2}\right)$ since the right side is strictly increasing as a function of λ and its values lie between $\tanh\left(\frac{2p_0}{\sqrt{-2p_0\gamma}}\right) < 0$ and ∞ if $\gamma > 0$, while for $\gamma < 0$ the monotonicity persists but we have to impose the condition $\lambda > 2p_0\gamma$ and on this interval the values range from $\frac{2p_0\gamma}{\tilde{g} - \gamma\sqrt{2p_0\gamma}} + \tanh\left(\frac{2p_0}{\sqrt{2p_0\gamma}}\right)$ to ∞ . Consequently, for the existence of a solution it is necessary, given $\gamma < 0$ and $p_0 < 0$, for \tilde{g} to be sufficiently large. Due to (2.4), this means that the absence of stagnation points is only granted for sufficiently large wavelengths.

Since it is known that the wave profile of a rotational travelling-wave in a flow of constant vorticity without stagnation points is real-analytic (see [9]), in principle one could pursue the above first-order considerations by expanding in powers series and identifying the coefficients at each order. Other than being a tedious exercise, such expansions are only granted locally and the determination of the radius of convergence seems out of reach especially since in the shallow-water regime (that is, for $d/L \ll 1$) the contribution of higher-order terms will tend to dominate so that results obtained by truncation at a certain order are only accurate for waves of small amplitude [6]. For these reasons we do not pursue a power series approach.

3.3 Bifurcation

The interpretation of the previous results in the space of solutions is provided by means of bifurcation theory: near the laminar flows (3.2), as the parameter λ varies, there are generally no genuine waves, except at critical values $\lambda = \lambda^*$ determined by the dispersion relation (3.15). Note that by (3.2) and (2.18), we have that $\sqrt{\lambda} = \frac{1}{H_p(0;\lambda)} = c - u(0,0)$, so that this result means that only critical values of the horizontal fluid velocity of the laminar flows at their flat free surface may trigger the appearance of waves. Near this bifurcating laminar flow H^* , we have two solution curves: one

laminar solution curve $\lambda \mapsto H(p; \lambda)$, where λ and Q are related by (3.3), and one non-laminar solution curve $Q \mapsto h(q, p; Q)$ such that $h_q \neq 0$ unless $h = H^*$. In [10] it was shown by means of a degree-theoretical approach (global bifurcation theory) that the local non-laminar solution curve can be extended to a global continuum \mathcal{C} that contains solutions of (2.19) with $\inf_{(q,p) \in R} \frac{1}{h_p(q,p)} \rightarrow 0$. This condition is characteristic of flows such that their horizontal velocity u is arbitrarily close to the wave speed c , at some point in the fluid, the limiting configuration being a flow with stagnation points. The global continuum \mathcal{C} comprises flows that are not small perturbations of a laminar flows, and therefore represent waves of large amplitude.

4 Optimization

In the following, we consider the numerical solution of the free boundary value problem for water waves with constant vorticity.

We propose a *Penalization Method* (PM) for solving the constraint optimization problem, to minimize

$$\mathcal{E}[h] := - \int_{-\pi}^{\pi} h_q^2(q, 0) dq, \quad (4.1)$$

subject to the PDE constraint that h satisfies (2.19). The energy functional \mathcal{E} is chosen in such a way that it vanishes for laminar flows (for which $h_q(\cdot, 0) \equiv 0$), thus selecting genuine waves with a non-flat free surface. Due to (2.17) and the second boundary condition in (2.7), we can relate the functional \mathcal{E} to the slope of the wave profile:

$$\mathcal{E}[h] = - \int_{-\pi}^{\pi} \eta_x^2(x) dx.$$

This is indicative of the fact that the proposed optimization problem selects waves of large amplitude. Note that the wave amplitude

$$a = \frac{\eta(0) - \eta(\pi)}{2} = \frac{1}{2} \int_0^{\pi} \eta_x(x) dx$$

satisfies $a^2 \leq -\frac{\pi}{8} \mathcal{E}[h]$. Also, since (2.1) can be re-stated in the form $\int_{-\pi}^{\pi} \eta(x) dx = 0$, Wirtinger's inequality [16] ensures

$$\int_{-\pi}^{\pi} \eta^2(x) dx \leq -\mathcal{E}[h].$$

We propose the following implementation the PM method:

1. Initialize $k = 0$: Choose a constant $\nu_0 > 0$ (typically small). Find an initial guess $h^{(0)}$ of the solution of (2.19). For initializing $h^{(0)}$ we select $h^{(0)}(q, p) = h^*(q, p; b)$ which gets the particular forms (3.10) and (3.12), for $\gamma = 0$ and $\gamma \neq 0$, respectively. These forms guarantee that (3.5) holds.

In order to calculate waves of large amplitude (one branch of the bifurcation is the laminar flow, and the other branch is the one with high amplitude), the particular choice of b is important for initialization: On the one hand the closer b is to 0, the smaller the residual is (cf. (3.5)). On the other hand for $b = 0$, $h^*(q, p; 0)$ is a laminar flow, and the PM algorithm is attracted to the laminar flow solution.

2. $k \rightarrow k + 1$: Given $h^{(k)}$ we solve the following linear equation for h , obtained by freezing the coefficients of lower order from the previous iteration step

$$\begin{aligned}
0 &= \mathcal{H}_l[h^{(k)}](h) \\
&= (1 + (h_q^{(k)})^2)h_{pp} - 2h_p^{(k)}h_q^{(k)}h_{pq} + (h_p^{(k)})^2h_{qq} + \gamma (h_p^{(k)})^3 \\
&\quad \text{in } R, \\
0 &= \mathcal{B}_{l,1}[h^{(k)}](h) \\
&= 1 + (h_q^{(k)})^2 + (2gh - Q)(h_p^{(k)})^2 \text{ for } p = 0, \\
0 &= \mathcal{B}_{l,2}[h^{(k)}](h) = h \text{ for } p = p_0.
\end{aligned} \tag{4.2}$$

The solution is denoted by $h^{(k+1)}$.

For the practical realization we used a 9-point difference scheme for the second derivative approximations of h_{pp} , h_{pq} , and h_{qq} . In particular, we use the central differences for h_{pp} and h_{qq} , we approximate the mixed derivative h_{pq} by

$$\begin{aligned}
&\frac{1}{6\Delta p \Delta q} [4h_{i-1,j} + 4h_{i+1,j} + 4h_{i,j-1} + 4h_{i,j+1} \\
&\quad + h_{i-1,j-1} + h_{i-1,j+1} + h_{i+1,j-1} + h_{i+1,j+1} - 20h_{i,j}]
\end{aligned}$$

and we use central difference quotients for h_p and h_q . We have chosen the number of discretization points in (q, p) directions as 60×60 , 40×40 , respectively. See Figure 9 and Figure 10.

3. Compute $h_p^{(k+1)}$. Because we work with a semi implicit scheme we have to use a relative small step-size, which is determined here.

- If $h_p^{(k+1)} > 0$ then put $\nu_{k+1} = \nu_k$ and update $h^{(k+2)}(q, p) = h^{(k+1)}(q, p) + \nu_{k+1} h_{qq}^{(k+1)}(q, p)$. We emphasize that $h_{qq}^{(k+1)}$ is the steepest descent energy of the quadratic functional \mathcal{E} . From this perspective we might call this algorithm a *steepest descent* algorithm.
- else put $\nu_{k+1} = 0$ and update

$$h^{(k+2)}(q, p) = F(p) - h^{(k)}(q, p).$$

The function F is given by $F(p) \simeq 2 \frac{d}{d^*} H^*(p)$ with d^* and d being the depths of $H^*(p)$ and $h^{(k)}(q, p)$, respectively. Using (2.16) we see that the depth d of a flow $h(q, p)$ can be computed by

$$d = \int_{-\pi}^{\pi} h(q, 0) dq.$$

4. Stopping criteria: The algorithm is terminated when the system of equations (2.19) is satisfied up to small error, i.e.,

- $\|\mathcal{H}_lh^{(k)}\| < \epsilon_1$ and $\|\mathcal{B}_{l,1}h^{(k)}\| < \epsilon_2$

and

- $\|h^{(k)} - h^{(k-1)}\| < \epsilon_3$, or
- $0 < 1/h_p^{(k)} < \epsilon_4$, which means that we are close to a stagnation point, i.e. $c - u = 1/h_p$ is positive and close to zero.

If the algorithm is not terminated then move to the second step.

Remark 1. *The parameter ν_0 has to be sufficiently small. Actually $\nu_k = \nu_0$ as long as $h_p^{(k+1)} > 0$. If this condition is violated the function $h^{(k)}$ is mirrored along $2d/d^* H^*(p)$ for different p . This transformation “inverts” the profile of the function $h^{(k)}$. Then the algorithm is continued with $\nu_k = 0$. This means that then a pure fixed point iteration (4.2) for (2.19) is realized. The first iteration steps with $\nu_k \neq 0$ move the approximation away from the laminar solution to the non-laminar solution.*

We are emphasizing that we are actually solving a PDE constraint optimization problem. They are typically saddle point problems, and therefore have a degenerate derivative, which a-priori prohibits for instance Newton’s

method. The standard numerical way to implement such problems are augmented Lagrangian methods, which perform descents in alternating directions. We have approximated the saddle point problem with a penalization method, which calculates a global minimizer, avoiding solving a saddle point problem. The steepest descent method is less efficient than Newton's method of course, however it is less sensitive to the choice of the initial guess. As one can see from Figure 2 the initial guess is a significant problem, which is even more pronounced with Newton's method.

In general, our algorithm consists of two parts. The first iterations should attract the approximations to the non-laminar solution. After the mirroring step, we are close to the non-laminar solution. The semi-implicit method (4.2) converges to the non-laminar solution of the PDE (2.19), which is the standard numerical approach for solving nonlinear PDEs in a stable way. Thus the first iterations are an auxiliary tool to find initial guesses for the fixed point iteration to converge to the non-laminar solution.

The different branches of the third step guarantee that the residuals of the boundary conditions and the differential equations are both decreasing. We have illustrated this for one example in Figure 2, where the necessity of changing the iteration becomes evident. More precisely, for the above algorithm, there is an iteration m that the condition $h_p^{(m+1)} > 0$ fails and we make the update $h^{(m+2)}(q, p) = F(p) - h^{(m)}(q, p)$. After performing one of these mirroring transformation steps the simulations show that for all $k = 1, \dots, m$

$$\|\mathcal{H}_lh^{(k)}\| < \|\mathcal{H}_lh^{(k-1)}\|$$

and

$$\|\mathcal{B}_{l,1}h^{(k)}\| > \|\mathcal{B}_{l,1}h^{(k-1)}\|,$$

as this is also depicted in Figure 2. For $k \geq m + 2$ we find that

$$\|\mathcal{H}_lh^{(k+1)}\| < \|\mathcal{H}_lh^{(k)}\|$$

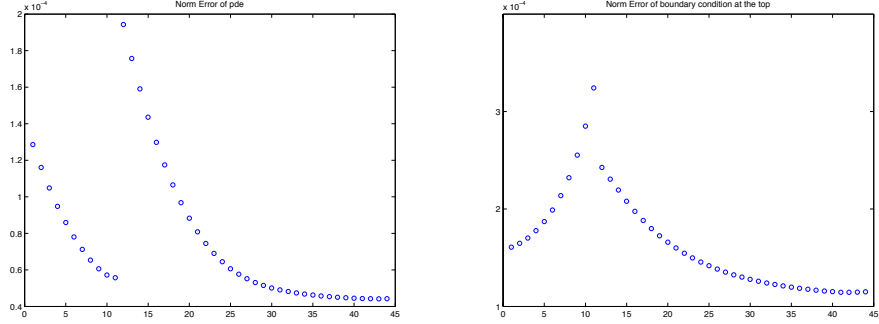
and

$$\|\mathcal{B}_{l,1}h^{(k+1)}\| < \|\mathcal{B}_{l,1}h^{(k)}\|,$$

as depicted in Figure 2. We illustrate the rate of convergence, after performing the mirroring in Figure 3.

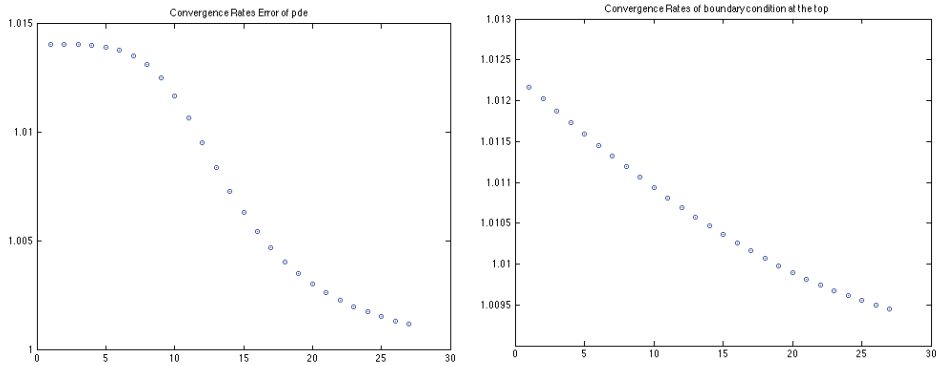
5 Results

We use that the gravitational constant $g = 9.8$ and we fix the relative mass flux $p_0 = -2$. We present the results of the numerical simulations for three



(a) The error of the PDE. (b) The error of the Boundary condition.

Figure 2: Numerical results for $\gamma = 0$. We have used 60×60 discretization points. The L_2 norms of the errors for the iterations (x -axis) for the boundary residual $\mathcal{B}_{l,1}$ and the equation residual \mathcal{H}_l .



(a) The quotient of the logarithm for the PDE. (b) The quotient of the logarithm for the Boundary condition.

Figure 3: Numerical results for $\gamma = 0$. The x -axis is counting the number of iterations. The quotient of the logarithm of the residuals for two successive iterations are depicted here. The fact that the quotients approach the value 1 from above indicates a linear convergence rate.

different cases:

- the irrotational case, $\gamma = 0$,
- the case of negative vorticity $\gamma = -2.95$,
- the case of positive vorticity $\gamma = 1$.

For all the cases we present the figures of

- the profile of the water wave, that is the free boundary S , (see Figure 4).
- the streamline pattern beneath the wave, that is the height $h(q, p)$ along the streamlines $p = -\psi$.
- the distribution of the vertical velocity v in the whole fluid, (see Figures 5, 6 and 7).
- the horizontal velocity $c - u$ on the vertical line below the crest, that is on the straight line segment $\{(q, p) : q = 0, p \in [p_0, 0]\}$, see Figure 8.
- the distribution of the pressure beneath the wave, see Figures 9 and 10.

Remark 2. *The numerical solution of the system (2.19) reveals increasing instabilities with decreasing values of γ . The problems might be due to instabilities in evaluation of the difference quotients. The increasing instability can be handled by decreasing the number of discretization points. This is why we could consider $\gamma = 0$ with a discretization of 60×60 and had to use just 40×40 for $\gamma = -2.95$. This also explains a spatial under-resolved visualization.*

6 Conclusion

In the present paper we proposed a penalization method for computing two-dimensional travelling water waves. We provided an iterative algorithm that starts with an approximation of a solution of the system (2.19) and converges to a solution which corresponds to a water wave of large amplitude. The formula of the initial approximation is given by (3.12) for the non-zero vorticity case; the irrotational case is given as a special case by simply substituting

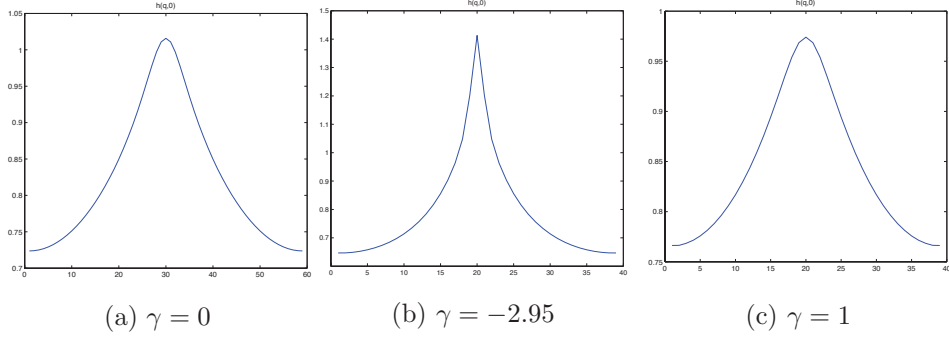


Figure 4: The periodic wave profile S . The x -axis (q -axis) is discretized into segments of length $2\pi/60$ for $\gamma = 0$ and $\gamma = 1$ and $2\pi/40$ for $\gamma = -2.95$. The numerical simulations indicate that for wave-current interactions in flows with negative vorticity the wave profiles present narrower crests and broader troughs than those in flows with non-negative vorticity, while in the latter cases the profile has reduced overall steepness. These features are confirmed experimentally (see [23]).

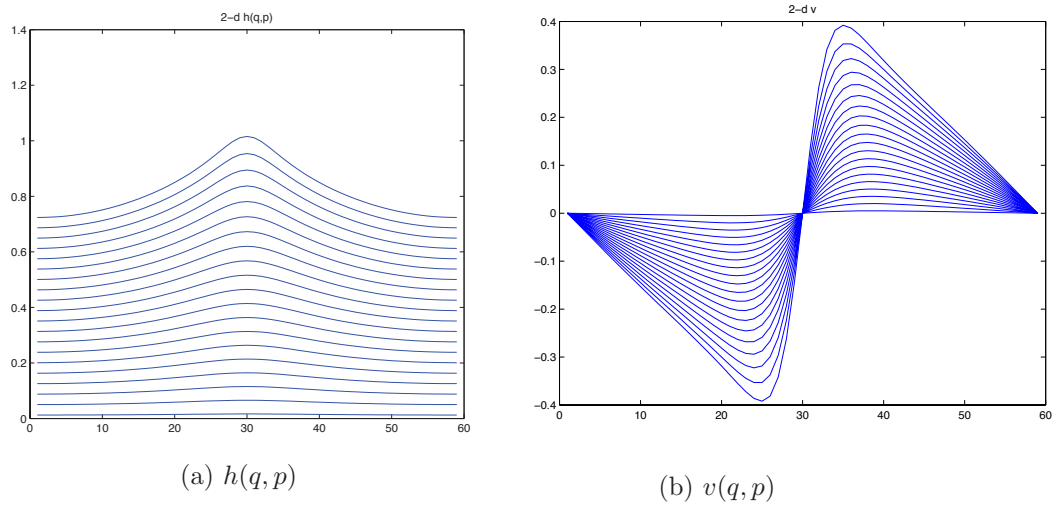


Figure 5: The height $h(q,p)$ of the streamlines and the vertical fluid velocity $v(q,p)$ along streamlines, depicted for the irrotational case $\gamma = 0$. The x -axis is discretized as described in Figure 4.

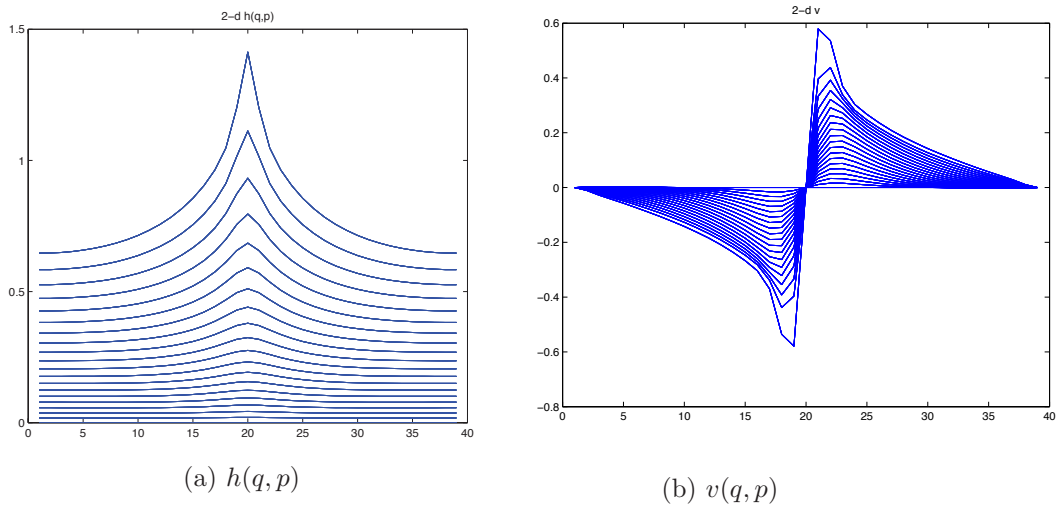


Figure 6: The height $h(q, p)$ of the streamlines and the vertical fluid velocity $v(q, p)$ along streamlines, depicted for the case $\gamma = -2.95$. The increased crest-trough asymmetry of the wave profile, due to a negative uniform vorticity distribution, is a feature that is replicated by all the streamlines above the flat bed (in the moving frame). The x -axis is discretized as described in Figure 4.

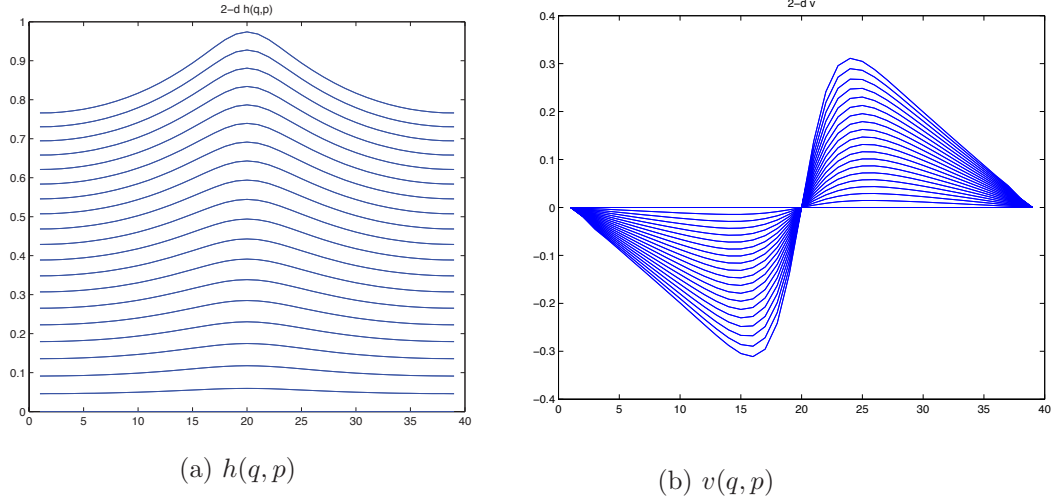


Figure 7: The height $h(q, p)$ of the streamlines and the vertical fluid velocity $v(q, p)$ along streamlines, depicted for the case $\gamma = 1$. The interaction with a current of positive vorticity produces a reduction of the overall wave steepness, compared with the case of an irrotational wave with no underlying current. This result is consistent with experimental investigations [23]. The x -axis is discretized as described in Figure 4.

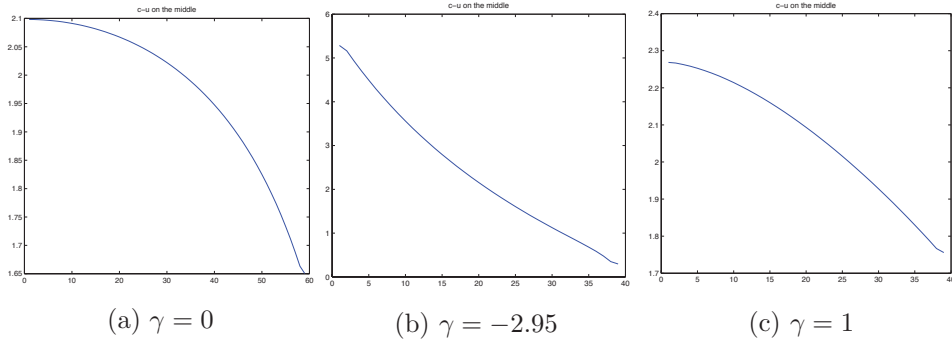


Figure 8: The horizontal fluid velocity $c - u$ beneath the wave crest, on the line segment $q = 0$. The presence of vorticity leads to significant changes of the velocity profile. The x -axis (p -axis) is discretized into segments of length $-p_0/60$ for $\gamma = 0$ and $\gamma = 1$ and $-p_0/40$ for $\gamma = -2.95$.

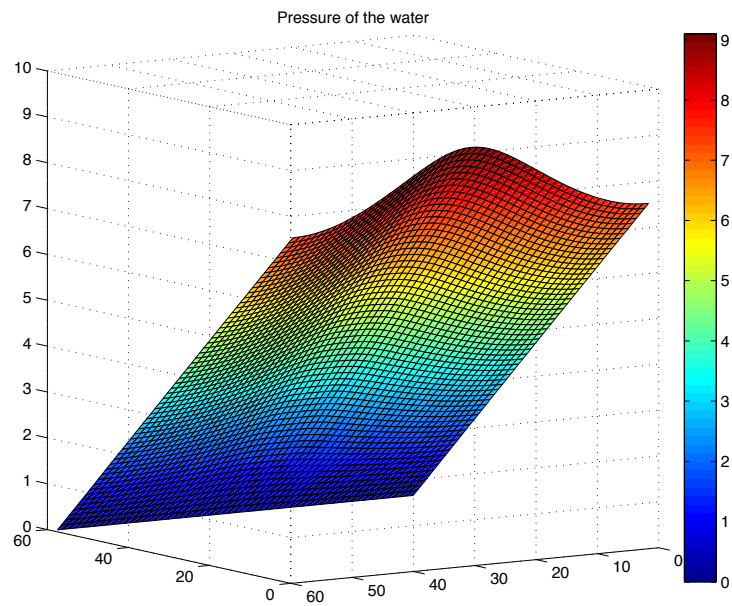


Figure 9: The pressure beneath the wave for $\gamma = 0$. The figure depicts the deviation of the pressure from the (constant) atmospheric pressure, $\mathbf{p} - P_{atm}$: vanishing at the free surface $p = 0$, it increases as we descend towards the flat bed $p = p_0$, the maximum being attained on the bed just below the wave crest (located in the middle of the horizontal segment for the discretization we have made).

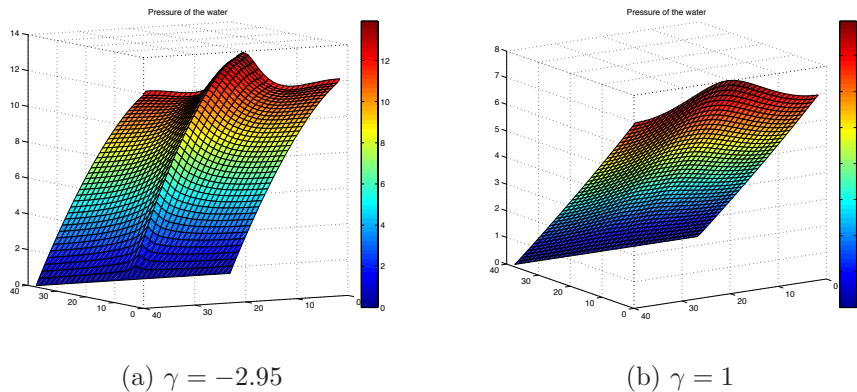


Figure 10: The pressure beneath rotational water waves. These results show that the sign of the vorticity plays a significant role. The pressure fluctuations at or near the seabed are of great practical relevance since they are frequently used to determine the wave conditions in shallow coastal waters (see the discussion in [7, 22]).

$\gamma = 0$. While we illustrate the case of constant vorticity, the approach can be implemented fairly easily for more general vorticity distributions.

Moreover, our pursuit for a better approximation of a non-laminar solution (which would serve the initial step of our iterative algorithm) has led to novel analytical results. In particular, explicit formulas that approximate non-laminar (large amplitude) travelling water waves with constant vorticity are obtained. The relevant analysis and formulas are to be presented in upcoming work.

Acknowledgements

The authors are grateful to both referees for constructive criticism and useful suggestions.

References

- [1] M. J. Ablowitz, A. S. Fokas and Z. H. Musslimani, On a new non-local formulation of water waves, *J. Fluid Mech.* **562** (2006), 313–343.
- [2] A. C. L. Ashton and A. S. Fokas, A non-local formulation of rotational water waves, *J. Fluid Mech.* **689** (2011), 129–148.

- [3] Y.-Y. Chen, H.-C. Hsu and G.-Y. Chen, Lagrangian experiment and solution for irrotational finite-amplitude progressive gravity waves at uniform depth, *Fluid Dyn. Res.* **42** (2010), Art. 045511 (34pp.).
- [4] D. Clamond, Note on the velocity and related fields of steady irrotational two-dimensional surface gravity waves, *Philos. Trans. Roy. Soc. London A* **370** (2012), 1572-1586.
- [5] A. Constantin, The trajectories of particles in Stokes waves, *Invent. Math.* **166** (2006), 523–535.
- [6] A. Constantin, *Nonlinear water waves with applications to wave-current interactions and tsunamis*, CBMS-NSF Conf. Ser. Appl. Math., Vol. 81, SIAM, Philadelphia, 2011.
- [7] A. Constantin, Estimating wave heights from pressure data at the bed, *J. Fluid Mech.* **743** (2014), R2, doi:10.1017/jfm.2014.81
- [8] A. Constantin, M. Ehrnström and E. Wahlén, Symmetry of steady periodic gravity water waves with vorticity, *Duke Math. J.* **140** (2007), 591–603.
- [9] A. Constantin and J. Escher, Analyticity of periodic traveling free surface water waves with vorticity, *Ann. of Math.* **173** (2011), 559–568.
- [10] A. Constantin and W. Strauss, Exact steady periodic water waves with vorticity, *Comm. Pure Appl. Math.* **57** (2004), 481-527.
- [11] A. Constantin and W. Strauss, Pressure beneath a Stokes wave, *Comm. Pure Appl. Math.* **53** (2010), 533–557.
- [12] A. Constantin, W. Strauss and E. Varvaruca, Global bifurcation of steady gravity water waves with critical layers, arXiv:1407.0092
- [13] A. Constantin and E. Varvaruca, Steady periodic water waves with constant vorticity: regularity and local bifurcation, *Arch. Ration. Mech. Anal.* **199** (2011), 33–67.
- [14] A. F. T. da Silva and D. H. Peregrine, Steep, steady surface waves on water of finite depth with constant vorticity, *J. Fluid Mech.* **195** (1988), 281–302.
- [15] M.-L. Dubreil-Jacotin, Sur la détermination rigoureuse des ondes permanentes périodiques d'amplitude finie, *J. Math. Pures Appl.* **13** (1934), 217–291.

- [16] H. Dym and H. P. McKean, *Fourier series and integrals*, Academic Press, New York-London, 1972.
- [17] L. Goddijn-Murphy, D. K. Woolf and M. C. Easton, Current patterns in the Inner Sound (Pentland Firth) from underway ADCP data, *J. Atmos. Ocean. Technol.* **30** (2013), 96–111.
- [18] I. G. Jonsson, Wave-current interactions, In *The Sea* (Ed. B. Le Méhauté and D. M. Hanes), J. Wiley & Sons, 1990, pp. 65–120.
- [19] J. Ko and W. Strauss, Effect of vorticity on steady water waves, *J. Fluid Mech.* **608** (2008), 197–215.
- [20] J. Ko and W. Strauss, Large-amplitude steady rotational water waves, *Eur. J. Mech. B Fluids* **27** (2008), 96–109.
- [21] A. Nachbin and R. Ribeiro-Junior, A boundary integral formulation for particle trajectories in Stokes waves, *Discrete Contin. Dyn. Syst.* **34** (2014), 3135–3153.
- [22] K. L. Oliveras, V. Vasan, B. Deconinck, and D. Henderson, Recovering the water-wave profile from pressure measurements, *SIAM J. Appl. Math.* **72** (2012), 897–918.
- [23] C. Swan, I. P. Cummins and R. L. James, An experimental study of two-dimensional surface water waves propagating on depth-varying currents, *J. Fluid Mech.* **428** (2001), 273–304.
- [24] G. P. Thomas, Wave-current interactions: an experimental and numerical study, *J. Fluid Mech.* **216** (1990), 505–536.
- [25] G. P. Thomas and G. Klopman, Wave-current interactions in the nearshore region, In *Gravity waves in water of finite depth* (Ed. J. N. Hunt), Adv. Fluid Mech., Vol. 10, 1997, pp. 215–319.
- [26] V. Vasan and K. Oliveras, Pressure beneath a traveling wave with constant vorticity, *Discrete Contin. Dyn. Syst.* **34** (2014), 3219–3239.
- [27] M. Umeyama, Eulerian-Lagrangian analysis for particle velocities and trajectories in a pure wave motion using particle image velocimetry, *Philos. Trans. Roy. Soc. London A* **370** (2012), 1687–1702.
- [28] J.-M. Vanden-Broeck, Steep solitary waves in water of finite depth with constant vorticity, *J. Fluid Mech.* **274** (1994), 339–348.

- [29] R. A. Walters, P. A. Gillibrand, R. G. Bell, and E. M. Lane, A study of tides and currents in Cook Strait, New Zealand, *Ocean Dyn.* **60** (2010), 1559–1580.